Experimental investigation of the electron energy distribution function (EEDF) by Thomson scattering and optical emission spectroscopy

Experimental investigation of the electron energy distribution function (EEDF) by Thomson scattering and optical emission spectroscopy

2012 J. Phys. D: Appl. Phys. 45 475202

(http://iopscience.iop.org/0022-3727/45/47/475202)

IOP PUBLISHING JOURNAL OF PHYSICS D: APPLIED PHYSICS

J. Phys. D: Appl. Phys. **45** (2012) 475202 (12pp) doi:10.1088/0022-3727/45/47/475202

Experimental investigation of the electron energy distribution function (EEDF) by Thomson scattering and optical emission spectroscopy

E A D Carbone[1], S Hübner[1], M Jimenez-Diaz[1], J M Palomares[1], E Iordanova[1], W A A D Graef[1], A. Gamero[2] and J J A M van der Mullen[1]

[1] Department of Applied Physics, Eindhoven University of Technology, PO Box 513, 5600 MB Eindhoven, The Netherlands

[2] Departamento de Fisica Aplicada, Universidad de Córdoba, Córdoba, Spain

E-mail: e.a.d.carbone@tue.nl

Received 10 June 2012, in final form 16 September 2012
Published 1 November 2012
Online at stacks.iop.org/JPhysD/45/475202

Abstract

The electron temperature of an argon surface wave discharge generated by a surfatron plasma at intermediate pressures is measured by optical emission spectroscopy (OES) and Thomson scattering (TS). The OES method, namely absolute line intensity (ALI) measurements gives an electron temperature which is found to be (more or less) constant along the plasma column. TS, on the other hand, shows a different behaviour; the electron temperature is not constant but rises in the direction of the wave propagation. In the pressure range of this study, it is theoretically known that deviations from Maxwell equilibrium are expected towards the end of the plasma column. In this paper, we propose a combination of methods to probe the electron energy distribution function (EEDF) in this relatively high-pressure regime. The ALI method combined with a collisional–radiative model allows one to measure the effective (Maxwellian) creation temperature of the plasma while TS measures the mean electron energy of the EEDF.

The differences between the two temperature methods can be explained by the changes in the form of the EEDF along the plasma column. A strong correlation is found with decreasing ionization degree for different pressures. Numerical calculations of the EEDF with a Boltzmann solver are used to investigate the departure from a Maxwellian EEDF. The relatively higher electron temperature found by TS compared with the ALI measurements is finally quantitatively correlated with the departure from a Maxwellian EEDF with a depleted tail.

(Some figures may appear in colour only in the online journal)

1. Introduction

Non-thermal plasmas generated at intermediate to high pressure (from a few mbars to atmospheric pressure and higher) have found a large number of applications in the last decades. They combine the advantages of large fluxes of active species (charged species, radicals and photons) while keeping non-destructive conditions for the substrate/environment. In the process of optimizing non-thermal plasmas, large ratio between the electron temperature T_e and the gas temperature T_h are often achieved. This large ratio, combined with a usually low ionization degree, implies that the conditions for which the electron energy distribution function (EEDF) is Maxwellian are rarely fulfilled. Depletion/overpopulation of the tail of the EEDF is commonly found, even for simple atomic plasmas [1–3]. In the case of gas mixtures, the EEDF can take even more complicated shapes where the distinction between a bulk and a tail temperature becomes itself doubtful [4–7].

In the case of high-pressure plasmas above a few torrs, classical diagnostic methods like Langmuir probes become

very difficult due to the collisional character of the sheath and an accurate and non-intrusive determination of the exact shape of the EEDF is very challenging [8, 9].

Time and space resolved optical emission spectroscopy (OES) has recently been used to probe the fast electrons of the EEDF for low-pressure capacitively coupled RF discharges. The RF, time-dependent, response of the fast electrons can be used to discriminate them from the slow electrons. Specific atomic lines sensitive to excitation from the ground state are then used as probe of the fast evolution of the tail of the EEDF due to the oscillating external E-field [10, 11].

Another recent method that was developed by different groups consists in the measurement of relative line emission intensities. The lines ratio is then linked to the EEDF via detailed collisional excitation and radiative losses particle balances [3, 12, 13]. This method can, in theory, determine the full shape of the EEDF but relies very strongly on the accuracy of the cross sections used in the collisional–radiative model (CRM), both in shape and in absolute value. Moreover, it requires an *a priori* knowledge of the shape of the EEDF to apply some multi-temperature iterative interpolation.

In this paper, we will follow a different approach. The absolute excited atomic states densities will be measured in order to determine the atomic state distribution function (ASDF). With the help of a CRM, the experimentally measured *excitation temperature* T_e^{ex} of the plasma will be corrected to determine the *creation temperature* T_e^{crea} of the plasma. The latter being determined as the effective Maxwellian electron temperature which is needed to sustain the creation of electron–ion (ei) pairs for given plasma conditions (see section 5.1 for more details). In the case of an argon plasma, this temperature is mostly determined by the shape of the tail of the EEDF as only highly energetic electrons can contribute to excitation and ionization processes from the ground state. On the other hand, the low-energy part of the EEDF is directly measured by Thomson scattering (TS). This experimental approach is equivalent to the 2-temperature EEDF approximation which is used in many analytical models, see for instance [1, 14, 15]. Consequently, this experimental method allows also keeping a relatively direct connection with the classical analysis (and prediction) of plasma properties which can be carried out via global plasma models (GPMs). This will be further discussed in section 5.2.

GPMs are often of great use for the characterization/understanding of plasmas. They are among others constructed to fulfil the dream of quasi-analytical expressions that predict internal plasma properties, such as the electron density, n_e, and temperature, T_e, as functions of the external plasma control parameters (the knobs) such as pressure, filling composition and plasma vessel size. To give a few examples of their use, in Lieberman and Lichtenberg classical textbook [16] several GPMs were discussed for low-pressure plasmas used in integrated circuits technology. In [17, 18] van de Sande *et al* gave an application to atmospheric inductively coupled plasmas used for spectrochemical analysis whereas in [19] a GPM was used to describe a low pressure, inductively coupled discharge lamp.

In the references mentioned above the plasma chemistry is quite simple; the plasmas are monoatomic, for instance created in pure argon or pure helium. The most simple GPMs usually consist of two balance equations; the electron particle balance (ePB) and the electron energy balance (eEB)[3]. In particular for the steady-state situation these balances are simple. It is remarkable that the ePB gives T_e whereas n_e follows from the eEB. Moreover, these two equations are only weakly coupled. In particular, the ePB, giving T_e is (almost) completely decoupled from the n_e-value in the case of purely diffusive plasmas [21][4].

The underlying reason is that, in steady state, T_e must attain the value for which the creation of ei pairs due to ionization compensates the losses generated by effluxes of ei pairs out of the active plasma zone. In this balance, both the creation and the effluxes scale with n_e, making the result n_e-independent.

Nowadays, numerous GPMs are developed to investigate plasma chemistry [24–27] whereas also time dependence is addressed [28]; as well as plasma interactions with electrodes/walls, e.g. the application of sputter plasmas [29].

In this study, we will investigate an intermediate pressure surface wave (SW) discharge. This plasma has the well-known properties of an electron density gradually decreasing along the wave propagation direction [30, 31]. Since the pressure and the plasma radius do not change along the column, one could expect, on ground of an ePB for a diffusive plasma, that T_e remains constant. This axial trend of a non-changing T_e was several times observed with OES applied to these types of plasmas (see for instance Lao *et al* [32]). Here, applying OES in the form of absolute line intensity (ALI) measurements combined with a CRM, we reported in the past the same tendency [33]. However, the T_e determined by TS applied to the same plasma conditions was found to follow a different behaviour [34]. This temperature, T_e(TS) is not constant but increases in the direction of decreasing n_e. Some theoretical papers predicted deviations from Maxwell equilibrium along the plasma column at low pressure [35, 36] or atmospheric pressure [37]. Lao *et al* [36] compared axial profiles of the 4s metastable and resonant excited argon atoms with the results of a self-consistent 1D model for pressures ranging between 0.5 and 2 Torr. They concluded that the observed rise in densities towards the end of the column could be reproduced by the model only while including non-Maxwellian excitation rates. Langmuir probe systems are very difficult to implement into a quartz tube because of the small radius of these SW discharges for pressures above a few hundreds Pa and they are a rather intrusive method for microwave plasmas. Consequently, very little experimental data exist about measurements of deviations from the Maxwell equilibrium. Dias *et al* [38] reported measurements of the EEDF for a low-pressure Ar/N_2 plasma. Tatarova *et al* [39, 40] measured with Langmuir probes the EEDF for an argon discharge with a large radius at low pressure for a few plasma conditions and a couple of positions.

[3] This system of two balance equations can be expanded by a third one, namely the heavy particle heat balance, see for instance [20] so that apart from n_e and T_e the gas temperature T_g can also be computed.

[4] In the opposite case, we refer for instance to the work of Aliev *et al* [22] for the influence of electron–electron recombination processes and Jonkers *et al* for molecular ions assisted recombination effects [23].

To the best of the author's knowledge, no actual experimental investigation of the EEDF was carried out for SW discharges with a radius below 5 mm and pressures above 5 mbar. In this study, we will investigate a SW discharge with a radius of 3 mm in a pressure range between 6 and 20 mbar.

It will be shown in this study that the discrepancy between the axial trend of T_e(ALI) and T_e(ePB) on one hand and that of T_e(TS) on the other hand, can be correlated with the change in the form of the EEDF for decreasing n_e values; or, better, as a function of the ionization degree $\alpha = n_e/N$ where N is the gas density.

This paper is organized as follows: the ePB for a low-pressure argon plasma in cylindrical coordinates is first briefly discussed. For intermediate pressure conditions, a SW plasma is first investigated by OES. The electron temperature is derived from ALI measurements combined with a CRM. The trends are first briefly discussed in terms of the ePB and then compared with TS measurements. The differences between the two diagnostics methods are finally discussed and investigated using a Boltzmann solver.

2. Effective ionization rate in an argon plasma

A central role in global plasma modelling is played by the ePB which for, steady state, diffusive plasmas reads [16]

$$n_e N k(T_e) = \nabla \cdot (D_a \nabla n_e) \tag{1}$$

expressing that ionization (lhs) compensates for diffusive losses of ei pairs (rhs). In this equation n_e and N are the densities of the electrons and ground state atoms, D_a is the coefficient for ambipolar diffusion whereas $k(T_e)$ is the *effective* rate coefficient for ionization from the ground state. Note that this equation is only valid in the case of a purely diffusive plasma, i.e. when there are no important losses or creation of electrons via volume recombination or other processes such as Penning ionization [41].

In the case of cylindrical plasmas, equation (1) can be simplified as

$$k(T_e) = D_a^* (N\Lambda_0)^{-2} \tag{2}$$

with $D_a^* = D_a N$ whereas Λ_0 stands for the effective diffusion length. In the case where the electron density profile follows a Bessel profile we can write for the diffusion length of electrons $\Lambda_0 = R/\mu$ for which R is the radius of the plasma and $\mu = 2.405$ the first zero of the J_0 Bessel function [16, 42]. In the case of argon, the ambipolar diffusion coefficient D_a for atomic ions is given by [43]

$$D_a \approx D_i \left(1 + \frac{T_e}{T_i}\right) = \frac{1}{3\sqrt{2} N \sigma_{ia}} \sqrt{\frac{8 k_B T_h}{\pi m_i}} \left(1 + \frac{T_e}{T_h}\right), \tag{3}$$

where m_i is the mass of the argon ion, σ_{ia} is the ion–atom collision cross section and is a weak function of the gas (ion) temperature. For argon at temperatures $T_h < 2000$ K, it can be approximated by the fit function [44]

$$\sigma_{ia} = 1 \times 10^{-18} + 1.5 \times 10^{-15} \times (\ln T_h)^{-3.9} \ (\mathrm{m}^2),$$

where T_h is expressed in (K). In this study, the T_h values were obtained via the ideal gas law $p = N k_B T_h$ for whom the gas density N was directly measured by Rayleigh scattering [45].

In the case of this SW discharge (radius of 3 mm), it was experimentally found that for pressures of 10 mbar and above, electrons are lost not only by diffusion but also by volume recombination through molecular ions Ar_2^+ [46]. Following the same reasoning as in [42], equation (2), can be rewritten as

$$k(T_e) = D_a^* (N\Lambda_0)^{-2} + k^{IC} N^2, \tag{4}$$

where the second term on the rhs stands for the extra ei pair losses by ion conversion followed by dissociative recombination. The ion conversion rate coefficient is given by $k^{IC} = 2.5 \times 10^{-43} (300/T_h)\ \mathrm{m}^6\ \mathrm{s}^{-1}$ [47].

The name *effective* rate coefficient for ionization, implies that $k(T_e)$ accounts for all kinds of electron-induced processes leading to ionization; direct ionization but also stepwise processes for which ionization is realized via intermediate excited states [48]. So, in general, $k(T_e)$ has to be determined by means of a CRM. For low electron density plasmas, (most) of the lower levels are ruled by the corona balance meaning that the excited levels are created by electron ground state excitation and lost by radiative decay (if the states are not metastable like the $^3P_2$ and $^3P_0$ levels of argon). Realizing that radiative decay obstructs ladder-like excitation, we can understand that only direct ionization leads to the creation of ei pairs. Thus for low n_e conditions, $k(T_e)$ can be replaced by $k^{dir}(T_e)$, the rate coefficient for direct ionization. For increasing n_e-values, radiative decay will be overruled by transitions driven by electron collisions and the corona balance makes place for the excitation saturation balance (ESB). It was shown [49–51] that for $n_e \gg 10^{19}\ \mathrm{m}^{-3}$ all excitation processes eventually lead to ionization and that therefore, the rate of effective ionization of argon is close to that of excitation, that is the formation of the 4s levels from the ground state. This especially holds when resonant radiations from the $^1P_1$ and $^3P_1$ back to the argon ground state are trapped.

From the summation over all excitation processes which effectively leads to ionization, an effective total ionization rate can be computed using a CRM, and fitted as a function of an effective Maxwellian temperature. In the electron density range considered here the following formula was proposed [52, 53]:

$$k(T_e) = k_{exc}(T_e) = 6.8 \times 10^{-17} T_e^{0.44} \exp(-12.06/T_e) \tag{5}$$

with T_e in eV.

Note that equation (2) which shows that T_e depends on the product RN, is the basis of a similarity's law often used in the field of microwave plasma studies [7, 54, 55]. The idea is that the electron temperature determined for one combination of R and N values can be attributed to other plasmas with similar properties, each with different R and N values, but having the same product RN.

3. Experimental setup and diagnostics

3.1. The plasma source

In this study, we will investigate a surfatron plasma belonging to the category of SW discharges. These plasmas are created

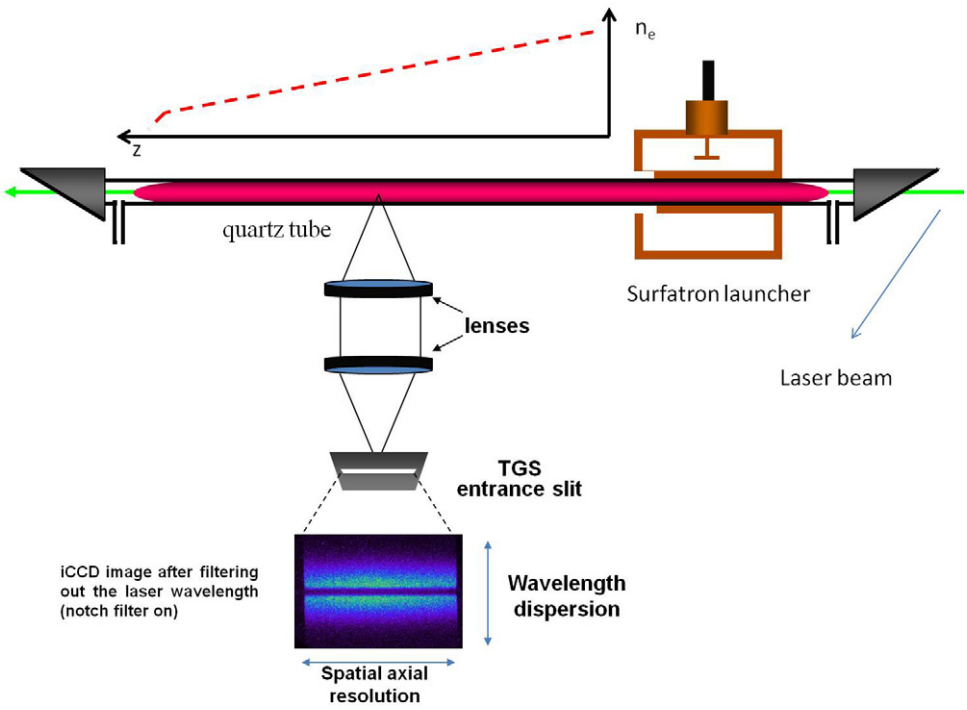

Figure 1. Schematic of the surfatron plasma source and the detection system for TS. In the case of the ALI measurements the triple grating spectrometer (TGS) is replaced by a standard single monochromator allowing to detect the argon emission lines [33].

by a launcher that generates an electromagnetic (EM) wave propagating at the interface between the quartz vessel wall and the plasma. Thus, the plasma makes the propagation possible so that the wave can transport EM energy to regions further away from the launcher where the plasma is sustained by the wave [56, 57].

Figure 1 gives a schematic of the surfatron setup. The edge of the launcher is taken as $z = 0$ and the wave propagates to the left; in the positive z-direction. Close to the launcher, the wave power content is large, so that the electron density created by the EM wave absorption is high as well. As the wave propagates it will loose energy so that the electron density drops along the wave. Since both R and N do not change dramatically along the wave, the ePB predicts that the effective electron temperature T_e remains almost constant (see section 4.1). The expected decrease in n_e and almost constant behaviour of T_e (i.e. ionization rate) makes SW plasmas an interesting case's studies for the investigation of departure from a Maxwellian EEDF.

3.2. ALI method

ALI measurements is basically a two-step approach. In the first step, the density η per statistical weight $\eta(3) = n(3)/g(3)$ of the 4p levels, briefly denoted as level 3 and the density of the ground state, level 1, is determined experimentally by ALI measurements [33] and Rayleigh scattering [45]. Their density compared with the one of the ground state $\eta(1) = N$ gives the excitation temperature T_{13}; the latter being determined by a Boltzmann exponent $\eta(3) = \eta(1)\exp(-E_{13}/k_B T_{13})$ so that

$$k_B T_{13} = E_{13}\left[\ln\frac{\eta(1)}{\eta(3)}\right]^{-1}. \qquad (6)$$

In the second step, a CRM [58, 59] is used to convert T_{13} into T_e. This is performed by employing the $r^1(3)$ coefficient to correct the Boltzmann expression into $\eta(3) = r^1(3)\eta(1)\exp(-E_{13}/k_B T_e)$. So that

$$k_B T_e = E_{13}\left[\ln\frac{\eta(1)}{\eta(3)} + \ln r^1(3)\right]^{-1}. \qquad (7)$$

This $r^1(3)$ coefficient, delivered by a CRM, depends, in general, on T_e and n_e. It accounts for the deviations from a Boltzmann distribution with respect to the ground state governed by T_e due to the non-local thermal equilibrium between the electrons and the heavy particles as well as radiation escape. This coefficient is determined from the CRM where all important production and loss mechanisms of some given states are included. We use here an updated cross sections database for the CRM [60] compared with the previous studies [33, 58, 61, 62]. The electron temperature obtained via this method is the effective Maxwellian temperature needed to sustain the excitation-ionization efflux through the argon excitation space. In the case of excited states densities which are governed by electrons both for excitation and de-excitation processes (i.e. in the so-called ESB), the dependence in n_e is expected to be weak [49]. It depends then mostly of the ground state density and the electron temperature [33].

3.3. Thomson scattering

TS is the scattering of (laser) light on free electrons. The photon flux in our experiment is generated by a frequency doubled Nd : YAG laser producing 100 mJ pulses of photons at $\lambda_0 = 532$ nm with a repetition rate of 10 Hz. The number of scattered photons is directly proportional to n_e, whereas the

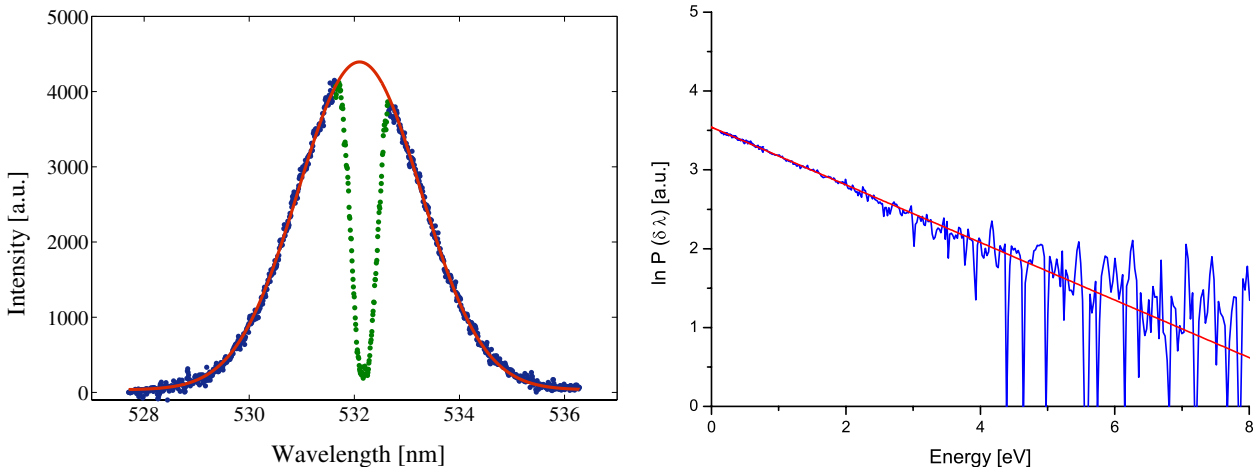

Figure 2. The number of counts $P(\delta\lambda)$ as a function of the wavelength shift $\delta\lambda = \lambda - \lambda_0$. Left: the measured $P(\delta\lambda)$ (experimental) fitted by a Gaussian superimposed on a base line. Right: the logarithm of $P(\delta\lambda)$ plotted versus $\delta\lambda^2$ shows, after baseline subtraction, the expected linear tendency for the first 7 nm^2. For higher $\delta\lambda$-values the noise obscures the signal.

Doppler broadening of the scattered photons gives insight in the electron energy distribution, and therewith T_e. This can be determined via the *1/e* width $\lambda_{1/e}$ [63] of the Gaussian distribution using the expression $T_e(\mathrm{TS}) = 5238 \cdot \lambda_{1/e}^2$. Another method is to analyse the Thomson scattered photons density $P(\delta\lambda)$ as a function of $\delta\lambda = \lambda - \lambda_0$. Since a Maxwellian EEDF leads to [64]

$$P(\delta\lambda) = A \exp\left(\frac{-m_e c^2 \delta\lambda^2}{4\lambda_0^2 k_B T_e}\right), \tag{8}$$

where A is a proportionality constant, c is the speed of light and λ_0 is the laser wavelength. In the case of a Maxwellian plasma, we may expect that a plot of $\ln P(\delta\lambda)$ versus $\delta\lambda^2$ gives a linear trend with a slope equal to $-1/k_B T_e$. This trend is indeed found for all the plasma conditions investigated in this study. Nevertheless, this can be directly checked only in the low electron energy range; above 4 eV the noise is obscuring the signal.

A typical TS spectrum is given in figure 2 as well as $\ln P(\delta\lambda)$ versus the electron energy. The intensity dip in the central region around $\delta\lambda = 0$ stems from the blocking of the signal around the central wavelength, i.e. at $\lambda = \lambda_0$; an action of the triple grating spectrometer (TGS) that is needed to reduce the influence of Rayleigh photons and false straylight which obscure the Thomson signal [64].

The scattering intensity decreases with $\delta\lambda$ and only the signal corresponding to relatively small $\delta\lambda$-values can be used to determine the electron temperature. The photon scattered distribution can only be constructed from the first 3 nm of wavelength shift $\delta\lambda$, which corresponds to electron kinetic energies up to 4.5 eV. Nevertheless, a simple integration shows that these electrons represent much more than 95% of the total population. Thus, we may state that TS gives the mean electron energy which conversely corresponds to the bulk temperature of the EEDF and that it does not provide information on the EEDF tail. Note that it is usually always the case for TS measurements. Information on the tail of the EEDF and, consequently, the creation temperature is directly obtained by TS only in the case when the assumption of a Maxwellian EEDF is valid. In the case of very large reactors, we shall mention the studies of Hori *et al* [65] and Crintea *et al* [66] who succeeded to probe under low-pressure conditions, the changes in the EEDF shape for energies up to ~10 eV for argon plasmas by TS. This is, however, still below the expected depletion threshold of the EEDF tail due to electron inelastic collisions (see figure 8 for instance). In that energy range, one should be, however, careful with systematic errors in the callibration of the detection system for the determination of the instrumental function of the TGS [64]. These errors will be minimized while using a rotationally resolved Raman spectrum for callibrating the spectrometer both in wavelength and intensity simultaneously [67]. In this study, a pure nitrogen gas at room temperature and fixed pressure was used. The fitting method was described in a previous paper [68].

4. Results

4.1. ALI results

In figure 3, the electron temperature obtained using the ALI-CRM method is shown for different pressures and the corresponding values from the ePB are given as a comparison. The latter are obtained with equation (4) in which we inserted $\Lambda_0 = R/\mu$ with $R = 3$ mm for the plasma radius meanwhile equation (5) is employed for $k(T_e)$.

One can see that the electron temperature obtained from ALI is found to be constant along the column within the error margins. The ePB gives a similar trend but with some differences in the quantitative aspects. For the lower pressure condition of 6 mbar, the electron temperature decreases slightly along the column. This is because of the decrease in the gas temperature (from 500 to 340 K) which leads to lower outwards ambipolar diffusion losses to the wall. On the other hand, for higher pressures, the behaviour is opposite. A slight increase in the electron temperature is found towards the end of the column. This effect comes from the formation of molecular

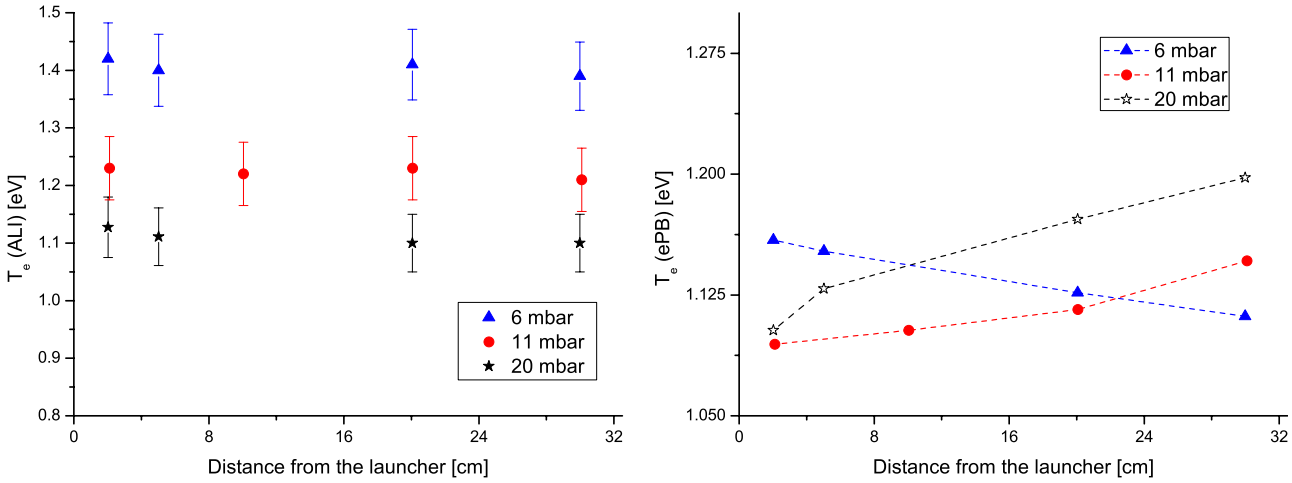

Figure 3. Electron temperature T_e(ALI) determined by ALI measurements along the plasma column for 6, 11 and 20 mbar. T_e(ALI) remains constant within the error margins for almost the entire plasma column. On the right, the electron temperature predicted by equation (4) is given under the same conditions. Note the difference in scales between the two pictures.

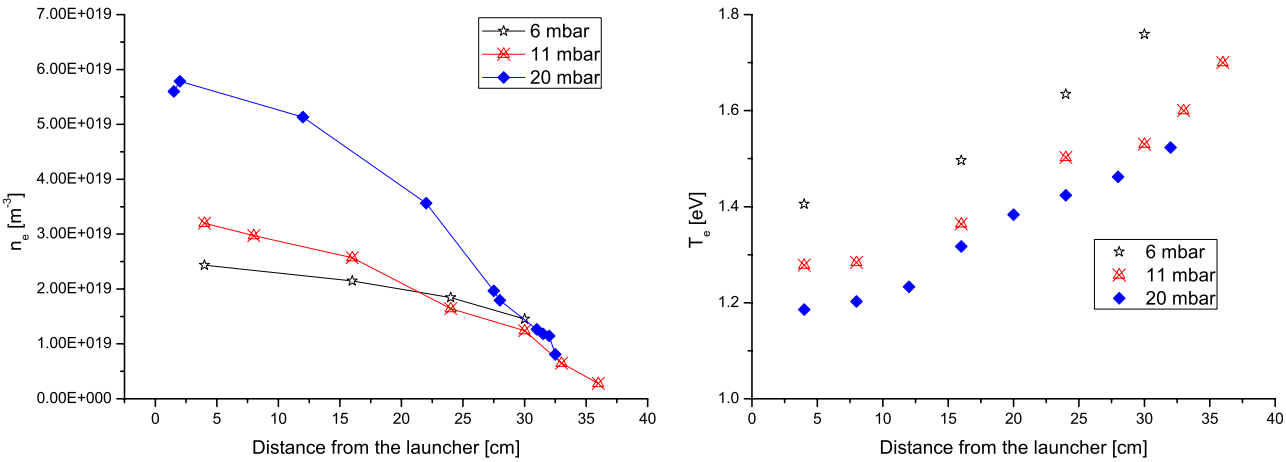

Figure 4. Electron temperature T_e measured by TS along the plasma column for different pressures. T_e(TS) is constant in the region close to the launcher and increase at the end of the column.

ions which increases the volume losses of ei pairs and induces a higher demand of electron temperature. Nevertheless, these trends predicted by the ePB are weak in terms of relative changes along the plasma column. The discrepancies between the ALI measurements and the predictions based on the simple ePB at lower pressure are actually larger than the changes due to the inhomogeneities (in neutral gas and molecular ions densities) along the plasma. The origin of the differences comes likely from the fit formula for the effective ionization formula. This fit formula was expected to be valid for plasmas with electron densities $10^{18} < n_e < 10^{20}\,\mathrm{m}^{-3}$ [53]. Nevertheless, the structure of equation (2) shows that excited species losses are implicitly assumed to come only by electron collisions; making this fit formula for the ionization rate from the CRM independent of n_e. This brings the assumption that the electron saturation balance is valid, so that radiative losses are negligible. This assumption is, however, doubtful under these plasma conditions, particularly in the lower pressure cases where the electron density is rather low with $n_e < 2 \times 10^{19}\,\mathrm{m}^{-3}$ (see figure 4). The electron saturation balance equilibrium is then not expected to be reached [69]. We will come back to the almost constant T_e axial trends in section 5 where the ALI and TS measurements will be compared and discussed.

4.2. TS results for T_e and n_e

For the same conditions as in the previous section, the electron temperature (and density) were measured by TS. The results, given in figure 4, show that, close to the launcher, the electron temperature values T_e(TS) as a function of pressure are very similar to the ones found by absolute line intensity measurements (T_e(ALI)). However, the axial trend is very different, in contrast to T_e(ALI), the T_e(TS) values are not constant along the column. In contrast, T_e(TS) increases in the direction of the wave propagation which corresponds to decreasing n_e values. Thus, we find that $\partial T_e/\partial n_e \ll 0$ rather than being approximately constant as for the ALI measurements. The rise along the plasma column is found to be steeper for higher pressures. It is interesting to note that, close to the launcher, T_e does not change much along the axis. Moreover, T_e(TS) is found be always larger than T_e(ALI) apart

in the region close to the launcher where the values are very close in absolute value to each other.

The increase found along the plasma column is actually much larger than the error bars due to the measurements. TS provides accurate values with relative errors below 5%. Systematic errors on T_e(TS) values are difficult to evaluate but expected to be quite small under these measurement conditions [42]. Discrepancies between the two methods due to the fact that the ALI measurements are averaged across the radius while TS gives only local values in the center cannot explain the trends either. In a previous study [42], we found, using TS, that the electron temperature is flat across the radius for pressures up to 20 mbar. Moreover, one would expect an increase in T_e towards the wall and consequently to find ALI values being higher than TS instead of being equal or lower. Radial gradients can be then neglected here and we can consider averaged quantities across the radius (i.e. use a GPM approach).

In the previous section, the effects of the molecular ion and the gas density profiles were already discussed based on the ePB and cannot explain the trends. In the next section, we will investigate the shape of the EEDF for different plasma conditions and discuss whether it can explain the trend of rising T_e(TS) along the plasma column. The discussion will be supported with calculations from a Boltzmann solver.

5. Discussion

5.1. Axial trends: correlation with the ionization degree along the column

In a recent study [57], a 2D self-consistent model was used to study a very similar surfatron configuration to the one used in this work. Effective Maxwellian rate coefficients were used and a flat electron temperature T_e was found both axially and radially for a pressure of 20 mbar. This confirms the results of the simple ePB (equation (4)), which showed that gas and molecular ions gradients along the plasma column do not significantly influence the electron temperature as long as effective Maxwellian rates are used. On the other hand, Benova *et al* [35] obtained theoretically an increasing mean electron energy along the plasma column for low-pressure SW discharges. This trend could be obtained only while taking the non-Maxwellian character of the plasma into account [36]. Unfortunately, the pressure range in these studies was always much lower than in the present one, so that no direct comparison can be made.

The axial trend in T_e(TS) found along the SW discharge is part of a larger category that can be denoted by the trend of rising T_e(TS) in outer plasmas parts. This was also observed experimentally in studies on atmospheric pressure plasmas (see for instance [17, 62, 68, 70, 71]) but also for low-pressure plasmas [38, 42]. In outer regions where n_e drops, the (mean) T_e values go up.

Compared with the intermediate pressure SW discharge investigated in this study, these atmospheric pressure plasmas have n_e-values that are a factor of about 50 larger; but the same factor more or less applies to the difference in the neutral gas density N. Consequently, similar behaviours for completely different plasmas sources and operation regimes (i.e. dielectric barrier discharge [71], radio-frequency [17] and microwave induced plasmas [68, 70]) are found for pressures above a few mbars. The common trend is the lower ionization degree towards the edges/end of the plasma.

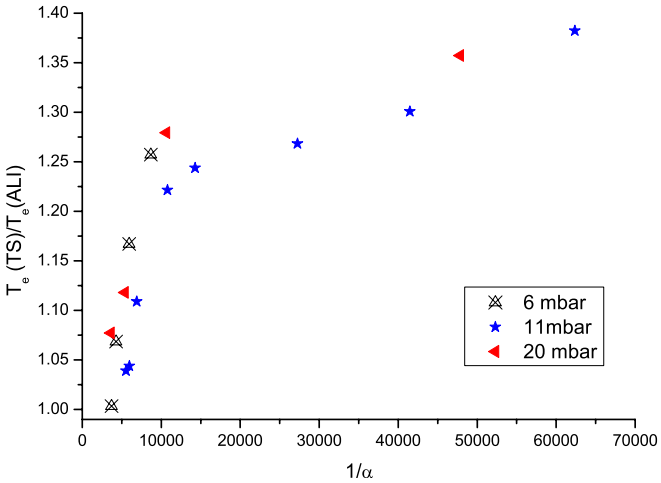

Figure 5. The ratio $\mathcal{R} = T_e(\text{TS})/T_e(\text{ALI})$ as a function for $\alpha^{-1} = N/n_e$ obtained experimentally for different pressures. The values follow a common trend which is an inverse function of the ionization degree of the plasma.

In order to find out whether the discrepancy between T_e(TS) and T_e(ALI) depends on the ionization degree we compare the ratio $\mathcal{R} = T_e(\text{TS})/T_e(\text{ALI})$ as a function of $\alpha = n_e/N$. The results, given in figure 5, are taken from the measurements presented in figures 3 and 4.

They show a common dependence; lower α-values lead to higher $\mathcal{R}$ ratios. Note here again that ALI is based on the assumption of a Maxwellian EEDF whereas TS measures the bulk electron temperature of the EEDF and do not give any direct information about the tail of the EEDF. This may suggest that the phenomenon of axially rising T_e(TS) is related to the departure of the local Maxwell equilibrium (LME). Indeed, in the case where the ionization degree is (too) low, the Coulomb collisions are not sufficient enough anymore to thermalize the upper part of the EEDF (see figure 6). TS gives insight in the bulk of the EEDF (from 0.2 to 4 eV) meanwhile the ALI measurements combined with the CRM [60] determine an effective Maxwellian electron temperature (i.e. the shape of the tail of the EEDF). The ratio between these two methods could be seen then as a measure of the depletion of the tail of the EEDF due to too little thermalization via Coulomb collisions.

In [52, 72, 73], studies of the effect of the ionization ratio $\alpha = n_e/N$ on the departure from the LME were presented. A criterion was found for the presence of LME setting a lower limit of ionization degree α for a Maxwellian plasma. LME is expected to be present if

$$\alpha \gg \alpha^{\text{crit}} \qquad \text{with } \alpha^{\text{crit}} = \frac{C(\text{Ar})}{2\ln\lambda_c}\left(\frac{k_B T_e}{E_{12}^*}\right)^2. \tag{9}$$

In the case of argon [52] we have $C(\text{Ar}) = 0.3$ and $E_{12}^* \approx 12$ eV. Inserting for the Coulomb logarithm $\ln\lambda_c = 7$ and $k_B T_e = 1.2$ eV we find that $\alpha^{\text{crit}} \approx 2 \times 10^{-4}$.

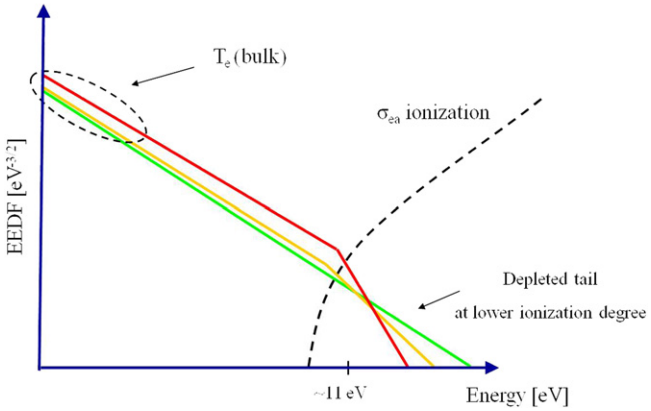

Figure 6. Schematic representation of the EEDF and the effective ionization cross section for ei pairs creation; small degrees of ionization will lead to a depleted tail's EEDF which as a response demands for an increase in the bulk electron temperature to keep a constant ionization rate.

Analysing figure 5, one can see that the temperature ratio $\mathcal{R}$ departs from 1 for ionization degrees which are indeed lower than this critical value ($1/\alpha > 5 \times 10^3$).

In the presentation of equation (2), it was assumed that the EEDF is Maxwellian and that for the computation of T_e, the Maxwellian formula for the effective ionization rate coefficient can be used; that is $k(\text{EEDF}) = k(T_e^M)$. But if the EEDF is non-Maxwellian we need another formula for $k(T_e)$, a formulation that no longer depends on just one single T_e-value but in principle on the whole EEDF. For moderate deviations from LME, this rate can be written as

$$k(\text{EEDF}) = k^M(T_e^{\text{bulk}})\, f(\alpha), \tag{10}$$

where the first factor at the rhs is the Maxwellian rate given by the bulk temperature (or mean energy), whereas $f(\alpha)$ gives a correction factor based on the departure from LME. In the case of plasmas with low reduced electric fields, this factor will mostly depend only on the ionization degree α.

So the ePB can be written as[5]

$$k^M(T_e^{\text{bulk}})\, f(\alpha) = \frac{D_a}{\Lambda_0^2 N}, \tag{11}$$

where the lhs takes the deviations from the Maxwell equilibrium into account by correcting the $k^M(T_e^{\text{bulk}})$ with the function $f(\alpha)$. This function has the property that a decreasing α leads to smaller $f(\alpha)$-values. The reason is that for lower α-values the Coulomb collisions between electrons are not able to compete with the loss of high-energy electrons by inelastic collisions as demanded by a Maxwellian rate. This leads to an EEDF with depleted tail. As depicted in figure 6 the resulting decrease in $f(\alpha)$ will demand higher T_e^{bulk}-values to keep the same $k(\text{EEDF})$ rate coefficient value. This is indeed the behaviour of $T_e(\text{TS})$ seen while moving in the direction of decreasing n_e and thus decreasing α. To keep an ei pairs creation at the same strength, an increasingly depleted EEDF tail need a correspondingly higher bulk temperature.

The fact that $T_e(\text{ALI})$ does not change (much) for decreasing α-values suggests that $T_e(\text{ALI})$ probes the efflux of ei pairs and is directly connected to the rhs of equation (2). This does not change much if we go along the plasma column towards lower n_e regions. In figure 3, the electron temperature profile predicted by the ePB is changing along the plasma column because of the non-homogeneous gas and molecular ion densities profiles. However, these effects are weak (± 0.1 eV). Therefore the 4p radiations, and thus T_{13}, probes the ionization efflux in the excitation space and thus the ei pair creation. So $T_e(\text{ALI})$ probes the creation of ei pairs and can be best defined as the *creation temperature of the plasma*: T_e^{crea}. Since its value is determined using a Maxwellian rate in the ePB balance

$$k^M(T_e^{\text{crea}}) = \frac{D_a^* N}{\Lambda_0^2}. \tag{12}$$

we come to the following definition: the creation temperature T_e^{crea} is the temperature that a Maxwellian electron gas would have in order to sustain the creation and to support the efflux of electron–ion (ei) pairs with the prescribed transport rate.

To resume the discussion about the axial trends, we may state that the discrepancy between the $T_e(\text{TS})$ and $T_e(\text{ALI})$ seems to be based on the departure from Maxwell equilibrium that comes in when the degree of ionization α becomes too low. For sufficiently high α-values for which the LME condition given in equation (9) is fullfilled, we would expect that $T_e^{\text{bulk}} = T_e^{\text{crea}}$ and so that $T_e(\text{TS}) = T_e(\text{ALI})$. This is indeed what was found in this study. For low α-values we find that $\mathcal{R} > 1$. The experimental ratio $\mathcal{R}$ is proposed as a tool to investigate the EEDF departure from a Maxwellian distribution. The validity of this proposition will be investigated in the next section while computing the EEDF with a Boltzmann solver for different plasma conditions.

5.2. Absolute electron temperature trends: comparison with the results of a Boltzmann solver

Now, after the discussion on the trends, we address the absolute differences between the electron temperature values. From the previous sections, it was found that in the case of this intermediate pressure SW discharge, the effective electron temperature T_e is defined by the total ionization rate needed to compensate for the ei pairs losses due to diffusion and volume recombination. This T_e value can be determined from the ePB given by equation (4) while using some fit formula from a CRM for the effective ionization rate coefficient.

Equation (5) was originally defined for argon plasmas close to the ESB [49] and so electron densities $n_e > 2 \times 10^{19}\ \text{m}^{-3}$. Indeed, it is for 20 mbar that the closest agreement between the ePB and the ALI T_e-values was found. At lower pressures, radiation escape leads to an increase in the losses which is not reflected in that simple ePB balance (i.e. effective ionization rate coefficient) but was included in the CRM used for the interpretation of the ALI measurements.

[5] Note that the following discussion is for purely diffusive plasmas. The extension of the ePB for plasmas where volume recombination and/or radiations losses are important is rather straightforward and will not be discussed here.

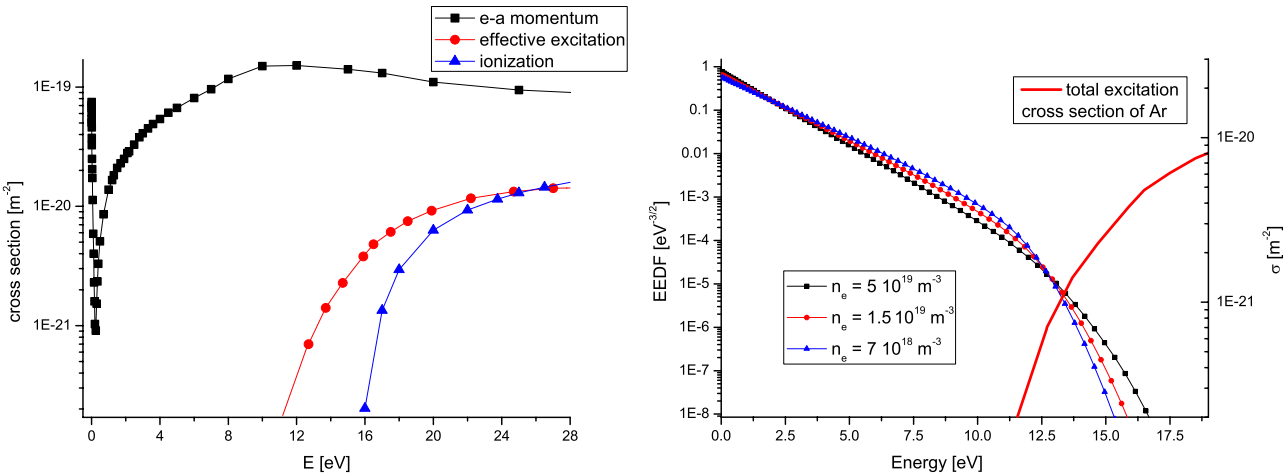

Figure 7. On the left, effective cross sections [75] used in Bolsig+ to calculate the deviations from the Maxwell equilibrium. On the right, the changes in the EEDF shape for an argon microwave plasma at 20 mbar are shown for different electron densities (i.e. ionization degree) and a constant total ionization rate coefficient of 1.9×10^{-19} m^3 s^{-1}.

To check whether the experimentally measured rise in the electron temperature corresponds directly to an increase in the mean electron energy (i.e. bulk temperature of the EEDF T_e^{bulk}) due to Maxwell deviations along the plasma column, we take a two-steps approach. First, the effective ionization rate as a function of the position along the plasma column is calculated from equation (4) while using the experimental T_e(ALI) values together with the gas density found by Rayleigh scattering under the same plasma conditions [45]. In a second step, the actual EEDF of the plasma was computed while solving the Boltzmann equation for the electrons in the approximation of a uniform electric field and two-terms expansion [74]. To do so, the freely available BOLSIG+ solver was used. For the computation of the EEDF, the experimental ionization degree, electron density and reduced angular frequency ω/N were used as input and the EEDF was obtained iteratively for various mean electron energies $\langle E \rangle$.

In figure 7, the shape of the EEDF as a function of the ionization degree for a fixed effective total ionization rate is given. The EEDF is indeed found to be Maxwellian up to 10 eV and the tail of the EEDF to be depleted. Moreover, for lower ionization degrees, the tail of the EEDF is found to be more depleted while the bulk temperature increases. In these calculations, direct ionization is found to be orders of magnitude lower than excitation towards the lumped 4s states, so that stepwise ionization is the dominant ionization process. Its corresponding rate coefficient was then directly taken as the effective ionization rate coefficient.

The expected bulk temperature of the EEDF T_e^{bulk} needed to produce the effective total ionization rate for a given plasma condition was then found while solving

$$k^M(T_e^{crea}(\text{ALI})) = k^{EEDF}(\alpha, n_e, \omega/N, \langle E \rangle) \qquad (13)$$

for the mean electron energy $\langle E \rangle$ with $T_e^{bulk} = 2/3\langle E \rangle$. The calculations were performed for the plasma at 20 mbar for which equation (5) can be directly used with the experimental creation temperature found by ALI. The results are shown in figure 8, the T_e^{bulk} temperature from BOLSIG+ is plotted

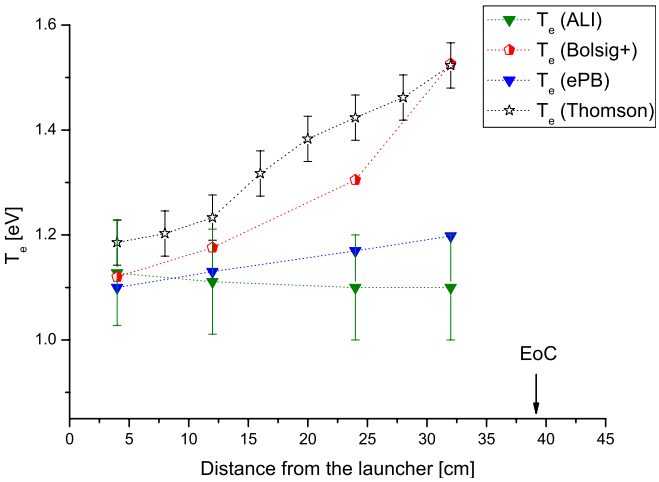

Figure 8. Comparison of the electron temperature obtained by TS and optical emission spectroscopy (ALI measurements) after correction for Maxwell deviations using a Boltzmann solver (BOLSIG+). The data presented here is for 20 mbar and compared with the prediction of the ePB.

versus the TS results along the plasma column. The electron temperatures obtained from the ePB and the ALI measurements are also shown for reference. A good agreement is found, both in trend and in absolute value. In the case of this intermediate pressure SW discharge, the temperature ratio $\mathcal{R}$ between the ALI and TS values, can be indeed correlated to the departure from a Maxwellian EEDF with a depleted tail. After correction for Maxwell deviations, the two experimental temperature methods (TS and ALI) agree within 0.1 eV.

In the cases where the dependence of the effective ionization rate as a function of a Maxwellian T_e is known (as given by equation (5) for instance), this iterative method can be used to correlate the so-called *creation temperature* of the plasma found by ALI with the real shape of the EEDF. Nevertheless, one needs to know plasma parameters such as the ionization degree and reduced electric field for these conditions

and can then use equation (13). In the case of plasmas with low reduced electric fields such as microwave plasmas, the knowledge of the mean electron energy $\langle E \rangle$ is enough on the other hand.

Small differences between the TS values and the ALI values corrected for deviations from Maxwell equilibrium remain but they are rather small. They might be attributed to uncertainties in the cross sections values used in the CRM as well as possible errors in the absolute callibration of the spectrometer for the ALI measurements. More detailed cross section sets could be also used for the calculations of the EEDF shape with the Boltzmann solver. Under some conditions, electron inelastic collisions with excited states of argon may change the shape of the EEDF at lower energies [74]. However, cumulative errors while comparing the two experimental methods are believed to be at least as important as the small differences found.

6. Conclusions and outlook

Global plasma models (GPMs) are very useful and handy tools in the classification and characterization of plasmas. They allow the calculation of important plasma quantities such as the electron temperature and density as well as the gas temperature. In the simple case of diffusive plasmas, the electron particle balance (ePB) can give the electron temperature in a way that does not depend (much) on the electron density. The ePB is, however, rather limited by the usual assumption of a Maxwellian distribution for the electrons. The experimental determination of deviations from the Maxwellian equilibrium and its link to the ePB, can then potentially largely increase the domain of validity of such GPMs.

In this study, we focused on an intermediate to high-pressure surface wave (SW) discharge where increasingly large deviations from the Maxwell equilibrium are expected down-wave the plasma column. A method for probing these deviations by active and passive plasma diagnostics, namely Thomson scattering (TS) and absolute line intensities (ALIs) measurements, is proposed. Using a Maxwellian distribution assumption, rather large discrepancies between these two methods are found towards the end of the plasma meanwhile they agree well close to the launcher. However, TS probes the low-energy electrons meanwhile ALI is an optical method which measures effectively the tail of the EEDF. The link with a change in the EEDF shape for decreasing n_e values is then made. In the case of this SW discharge, the ionization degree is found to play an important role and its effect can be linked back to the GPM formalism.

To label the temperature found by these two methods we use the name creation temperature T_e^{crea}: the temperature needed for Maxwellian electron gas to create the plasma with a prescribed creation ability. TS on the other hand delivers the bulk temperature T_e^{bulk} of the EEDF.

Using a Boltzmann solver, the link between the creation temperature found by ALI and the bulk temperature measured by Thomson scattering is done via the shape of the EEDF. A very good agreement is found provided that the dependence of the effective ionization rate from the ground state is known as a function of the (Maxwellian) *creation temperature* of the plasma. The latter needs to be determined via a CRM for a prescribed range of electron densities and pressures. We confined ourselves to the case where the electron saturation balance limit ($n_e > 2 \times 10^{19}\,m^{-3}$) is expected to be valid. The mean electron energy predicted by the Boltzmann solver is found to agree closely with the electron temperature found by Thomson scattering.

In the last couple of years some new optical methods based on CRMs are being developed. Instead of using absolute measurements, they are based on the measurement of intensity ratio of specific atomic lines [76] or combination of lines intensities of an atom [12, 13] or atomic lines from different species [77, 78]. These methods might replace the ALI-CRM procedure and make the tasks of the experimentalist simpler. Working with relative line intensities (RLI-CRM) instead of absolute line intensities (ALI) is easier since the complicated absolute calibration step can be skipped. An accompanying by-coming advantage of these RLI-CRM methods could be that apart from the electron temperature, the EEDF shapes can also be obtained. Nevertheless, these techniques are very sensitive to the cross sections datasets used as input of the CRM. Also, special care needs to be taken for radiation trapping effects which may strongly depend on spatial inhomogenieties of the lower levels involved in the radiative de-excitation processes. Overcoming the limitations of a Maxwellian temperature in the ALI method seems then still a promising method for plasma diagnostics. Indeed, all uncertainties in callibration and cross sections will be largely reduced in the logarithmic dependence of T_e with the species densities (i.e. 4p states) and cross sections used (included in the r^1-coefficients).

Different (quasi-) analytical models exist in the litterature [1, 15, 79] which can be used to extend the description of non-Maxwellian plasmas in terms of two or more electron temperatures. Such refined models could be used to obtain a more detailed relation between plasma parameters such as the ionization degree α and departure from equilibrium and being used for the validation of reaction rates used in CRMs. This is, however, beyond the scope of this study.

Acknowledgments

This work is supported and financed by the Dutch Technology Foundation STW under the project numbers 10744 and 10497. One of the authors, EC, would also like to thank professor Nader Sadeghi for stimulating discussions.

References

[1] Cherrington B 1979 *IEEE Trans. on Electron Devices* **26** 148
[2] Gould R J and Thakur R K 1971 *Phys. Fluids* **14** 1701
[3] Zhu X M, Chen W C, Li J, Cheng Z W and Pu Y K 2012 *Plasma Sources Sci. Technol.* **21** 045009
[4] Behringer K and Fantz U 1994 *J. Phys. D: Appl. Phys.* **27** 2128
[5] Hartgers A, van Dijk J, van der Heijden H W P and van der Mullen J A M 2003 *J. Phys. D: Appl. Phys.* **36** 2269

[6] Bazhenov V, Ryabtsev A, Soloshenko I, Terent'eva A, Khomich V, Tsiolko V and Shchedrin A 2001 *Plasma Phys. Rep.* **27** 813

[7] Ferreira C, Alves L, Pinheiro M and Sa A 1991 *IEEE Trans. on Plasma Science* **19** 229

[8] Godyak V A, Piejak R B and Alexandrovich B M 2002 *Plasma Sources Sci. Technol.* **11** 525

[9] Godyak V A and Demidov V I 2011 *J. Phys. D: Appl. Phys.* **44** 233001

[10] Gans T, Schulz-von der Gathen V and Döbele H F 2004 *EPL Europhys. Lett.* **66** 232

[11] Schulze J, Schüngel E, Donkó Z, Luggenhölscher D and Czarnetzki U 2010 *J. Phys. D: Appl. Phys.* **43** 124016

[12] Boffard J B, Jung R O, Lin C C and Wendt A E 2010 *Plasma Sources Sci. Technol.* **19** 065001

[13] Boffard J B, Jung R O, Lin C C, Aneskavich L E and Wendt A E 2011 *Plasma Sources Sci. Technol.* **20** 055006

[14] Lichtenberg A J, Vahedi V, Lieberman M A and Rognlien T 1994 *J. Appl. Phys.* **75** 2339

[15] Maya J and Lagushenko R 1989 *Advances in Atomic, Molecular and Optical Physics* vol 26 ed D Bates and B Bederson (New York: Academic) p 321

[16] Lieberman M A and Lichtenberg A J 2005 *Principle of Plasma Discharges and Material Processing* (New York: Wiley)

[17] Van de Sande M, Van Eck P, Sola A and Van der Mullen J 2002 *Spectrochim. Acta* B **57** 829

[18] van de Sande M, van Eck P, Sola A, Gamero A and van der Mullen J 2003 *Spectrochim. Acta* B **58** 783

[19] Jonkers J, Van Dijk J and Van Der Mullen J 1999 *J. Phys. D: Appl. Phys.* **32** 898

[20] Broks B H P and van der Mullen J J A M 2006 *J. Phys. Conf. Ser.* **44** 53

[21] Zhelyazkov I and Atanassov V 1995 *Phys. Rep.* **255** 79

[22] Aliev Y M, Grosse S, Schluter H and Shivarova A 1996 *Phys. Plasmas* **3** 3162

[23] Jonkers J, Sande M V D, Sola A, Gamero A, Rodero A and Mullen J van der 2003 *Plasma Sources Sci. Technol.* **12** 464

[24] Gudmundsson J T, Marakhtanov A M, Patel K K, Gopinath V P and Lieberman M A 2000 *J. Phys. D: Appl. Phys.* **33** 1323

[25] Kim S, Lieberman M A, Lichtenberg A J and Gudmundsson J T 2006 *J. Vac. Sci. Technol.* A **24** 2025

[26] Thorsteinsson E G and Gudmundsson J T 2010 *Plasma Sources Sci. Technol.* **19** 015001

[27] Despiau-Pujo E and Chabert P 2009 *Plasma Sources Sci. Technol.* **18** 045028

[28] Lieberman M and Ashida S 1996 *Plasma Sources Sci. Technol.* **5** 145

[29] Gudmundsson J T 2008 *J. Phys. Conf. Ser.* **100** 082013

[30] Schluter H and Shivarova A 2007 *Phys. Rep.* **443** 121

[31] Moisan M and Zakrzewski Z 1991 *J. Phys. D: Appl. Phys.* **24** 1025

[32] Lao C, Cotrino J, Palmero A, Gamero A and González-Elipe A 2001 *Eur. Phys. J. D: At. Mol. Opt. Plasma Phys.* **14** 361

[33] de Vries N, Iordanova E, Hartgers A, v Veldhuizen E M, v d Donker M J and v d Mullen J J A M 2006 *J. Phys. D: Appl. Phys.* **39** 4194

[34] Palomares J, Iordanova E, van Veldhuizen E, Baede L, Gamero A, Sola A and van der Mullen J 2010 *Spectrochim. Acta* B **65** 225

[35] Benova E, Petrova Ts, Blagoev A and Zhelyazkov I 1998 *J. Appl. Phys.* **84** 147

[36] Lao C, Gamero A, Sola A, Petrova T, Benova E, Petrov G M and Zhelyazkov I 2000 *J. Appl. Phys.* **87** 7652

[37] Pencheva M, Petrova T, Benova E and Zhelyazkov I 2006 *J. Phys. Conf. Ser.* **44** 110

[38] Dias F M, Tatarova E and Ferreira C M 1998 *J. Appl. Phys.* **83** 4602

[39] Tatarova E and Zamfirov D 1995 *J. Phys. D: Appl. Phys.* **28** 1354

[40] Grosse S, Schlter H and Tatarova E 1994 *Phys. Scr.* **50** 532

[41] Penning F M 1927 *Naturwissenschaften* **15** 818

[42] Carbone E A D, Hübner S, Palomares J M and van der Mullen J J A M 2012 *J. Phys. D: Appl. Phys.* **45** 345203

[43] Mitchner M and Kruger C H 1973 *Partially Ionized Gases* (New York: Wiley)

[44] Phelps A V 1994 *J. Appl. Phys.* **76** 747

[45] Hübner S, Iordanova E, Palomares J, Carbone E and van der Mullen J 2012 *Eur. Phys. J. Appl. Phys.* **58** 20802

[46] Hübner S, Palomares J M, Carbone E A D and van der Mullen J J A M 2012 *J. Phys. D: Appl. Phys.* **45** 055203

[47] Hawley M and Smith M A 1992 *J. Chem. Phys.* **96** 326

[48] Simpson S W 1990 *J. Phys. D: Appl. Phys.* **23** 1161

[49] van der Mullen J A M 1990 *Phys. Rep.* **191** 109

[50] van der Mullen J and Jonkers J 1999 *Spectrochimica Acta* B **54** 1017

[51] de Vries N, Palomares J M, van Harskamp W J, Iordanova E I, Kroesen G M W and van der Mullen J J A M 2008 *J. Phys. D: Appl. Phys.* **41** 105209

[52] van der Mullen J A M and Jonkers J 1999 *Spectrochim. Acta* B **54** 1017–44

[53] de Vries N 2008 Spectroscopic study of microwave induced plasmas *PhD Thesis* Eindhoven University of Technology

[54] Ferreira C M and Moisan M 1988 *Phys. Scr.* **38** 382

[55] Ferreira C M 1983 *J. Phys. D: Appl. Phys.* **16** 1673

[56] Aliev Y M, Schlüter H and Shivarova A 1999 *Guided-Wave-Produced Plasmas* (Berlin: Springer)

[57] Jimenez-Diaz M, Carbone E A D, van Dijk J and van der Mullen J J A M 2012 *J. Phys. D: Appl. Phys.* **45** 335204

[58] Benoy D, van der Mullen J, Sijde B V D and Schram D 1991 *J. Quant. Spectrosc. Radiat. Transfer* **46** 195

[59] Hartgers A, van Dijk J, Jonkers J and van der Mullen J 2001 *Comput. Phys. Commun.* **135** 199

[60] Graef W A A D 2012 Zero-dimensional models for plasma chemistry *PhD Thesis* Eindhoven University of Technology

[61] Iordanova E, Palomares J M, Gamero A, Sola A and van der Mullen J J A M 2009 *J. Phys. D: Appl. Phys.* **42** 155208

[62] Palomares J M, Iordanova E I, Gamero A, Sola A and v d Mullen J J A M 2010 *J. Phys. D: Appl. Phys.* **43** 395202

[63] Uhlenbusch H K J 2000 *Plasma Sources Sci. Technol.* **9** 492

[64] van de Sande M J 2002 Laser scattering on low temperature plasmas: high resolution and straylight rejection *PhD Thesis* Eindhoven University of Technology

[65] Hori T, Kogano M, Bowden M D, Uchino K and Muraoka K 1998 *J. Appl. Phys.* **83** 1909

[66] Crintea D L, Czarnetzki U, Iordanova S, Koleva I and Luggenhölscher D 2009 *J. Phys. D: Appl. Phys.* **42** 045208

[67] Howard J, James B W and Smith W I B 1979 *J. Phys. D: Appl. Phys.* **12** 1435

[68] van Gessel A F H, Carbone E A D, Bruggeman P J and van der Mullen J J A M 2012 *Plasma Sources Sci. Technol.* **21** 015003

[69] van der Mullen J, van der Sijde B and Schram D 1980 *Phys. Lett.* A **79** 51

[70] van der Mullen J, van de Sande M, de Vries N, Broks B, Iordanova E, Gamero A, Torres J and Sola A 2007 *Spectrochim. Acta* B **62** 1135

[71] Tomita K, Bolouki N, Shirozono H, Yamagata Y, Uchino K and Takaki K 2012 *J. Instrum.* **7** C02057

[72] Hartgers A and van der Mullen J A M 2001 *J. Phys. D: Appl. Phys.* **34** 1907

[73] van der Mullen J and Broks B 2006 *J. Phys. Conf. Ser.* **44** 40

[74] Hagelaar G J M and Pitchford L C 2005 *Plasma Sources Sci. Technol.* **14** 722

[75] Yanguas-Gil Á, Cotrino J and Alves L L 2005 *J. Phys. D: Appl. Phys.* **38** 1588
[76] Boffard J B, Jung R O, Lin C C, Aneskavich L E and Wendt A E 2012 *J. Phys. D: Appl. Phys.* **45** 045201
[77] Zhu X M and Pu Y K 2011 *Plasma Sci. Technol.* **13** 267
[78] Zhu X M, Pu Y K, Celik Y, Siepa S, Schüngel E, Luggenhölscher D and Czarnetzki U 2012 *Plasma Sources Sci. Technol.* **21** 024003
[79] Gudmundsson J T 2001 *Plasma Sources Sci. Technol.* **10** 76